Journal of Power Sources 189 (2009) 966–971

Contents lists available at ScienceDirect

Journal of Power Sources

journal homepage: www.elsevier.com/locate/jpowsour

(Titanium, chromium) nitride coatings for bipolar plate of polymer electrolyte membrane fuel cell

H.S. Choi*, D.H. Han, W.H. Hong, J.J. Lee

Department of Materials Science and Engineering, Seoul National University, San 56-1, Silim-dong, Kwanak-gu, Seoul, 151-742, South Korea

ARTICLE INFO

Article history:
Received 16 September 2008
Received in revised form
20 November 2008
Accepted 1 December 2008
Available online 25 December 2008

Keywords:
Bipolar plate
Polymer electrolyte membrane fuel cell
Corrosion
Interfacial contact resistance
(Titanium, chromium) nitride

ABSTRACT

(Titanium, chromium) nitride [(Ti,Cr)N] coatings are synthesized on a 316L stainless-steel substrate by inductively-coupled, plasma-assisted, reactive direct current magnetron sputtering. The chemical and electrical properties of the coating are investigated from the viewpoint of it application to bipolar plates. Nanocrystallized Cr–Ti films are formed in the absence of nitrogen gas, while a hexagonal β-$(Ti,Cr)_2N$ phase is observed at N_2 = 1.2 sccm. Well-crystallized (Ti,Cr)N films are obtained at N_2 > 2.0 sccm. The corrosion resistance of the coating is examined by potentiodynamic and potentiostatic tests in 0.05 M H_2SO_4 + 0.2 ppm HF solution at 80 °C, which simulates the operation conditions of a polymer electrolyte membrane fuel cell. The Davies method is used to measure the interfacial contact resistance between the sample and carbon paper. The (Ti,Cr)N coating exhibits the highest corrosion potential and lowest current density. In a cathode environment, the corrosion potential and current density are 0.33 V (vs. SCE) and $<5 \times 10^{-7}$ A cm^{-2} (at 0.6 V), respectively. In an anode environment the corresponding values are 0.16 V and $<-5 \times 10^{-8}$ A cm^{-2} at −0.1 V. The (Ti,Cr)N coatings exhibit excellent stability during potentiostatic polarization tests in both anode and cathode environments. The interfacial contact resistance decreases with deposition of the (Ti,Cr)N film, and a minimum value of 4.5 mΩ cm^2 is obtained at a compaction force of 150 N cm^{-2}, which indicates that the formation of oxide films can be successfully prevented by the (Ti,Cr)N film. Analysis with Auger electron spectroscopy reveals that the oxygen content at the surface decreases with increase in the nitrogen content.

1. Introduction

Recently, polymer electrolyte membrane fuel cells (PEMFCs) have attracted considerable attention in the automobile industry on account of their high power density, low emissions, and low operating temperature [1–4]. A key determinant of the commercial realization of PEMFCs is the bipolar plate; this component accounts for most of the total weight and cost of the PEMFC stack [5,6]. The material requirements for a bipolar plate are high electrical conductivity, high corrosion resistance, low gas permeability, low weight, easy machining, and low cost. Stainless-steel is considered to be one of the most promising candidate materials that can be used as a bipolar plate instead of graphite because of its high electrical and thermal conductivity, ductility, low gas permeability, and low manufacturing cost. On the other hand, stainless-steel bipolar plates exhibit low corrosion resistance in the acidic environment that is typically present in fuel cells. The corrosion of stainless-steel leads to the formation of a passive oxide film on its surface that increases the interfacial contact resistance and degrades the fuel cell performance.

Surface modification by the thermal nitrification method is one of the solutions to this corrosion problem [7–12]. Brady et al. [11] reported that thermal nitrification (24 h at 1100 °C) of stainless-steel and a nickel–chromium-based alloy is useful for manufacturing bipolar plates. It was found that the Cr–nitride surface layer formed on Cr–Ni-based alloys exhibited excellent corrosion resistance and low interfacial contact resistance under simulated PEMFC bipolar-plate conditions. Unfortunately, however, thermal nitrification generally requires a high-temperature process (>1000 °C) that can cause undesirable deformation of the machined metal bipolar plate [13,14] and can decrease of corrosion resistance [15,16]. Further, the process typically entails a high manufacturing cost.

Coating the metal bipolar plate with a conductive polymer [17], carbon [18,19], a novel metal [20], a metal nitride [21–26], or a conductive oxide [27,28] is another method that is used to increase the corrosion resistance and decrease the contact resistance. Among the options, transition metal nitrides, especially TiN, have attracted considerable interest due to their high chemical stability and conductivity. For instance, Myung et al. [25] investigated the electrophoretic deposition of a coating of TiN nanoparticles with elastic

* Corresponding author. Tel.: +82 2 880 5511; fax: +82 2 871 5540.
E-mail address: nalbazu5@hotmail.com (H.S. Choi).

0378-7753/$ – see front matter © 2008 Elsevier B.V. All rights reserved.
doi:10.1016/j.jpowsour.2008.12.060

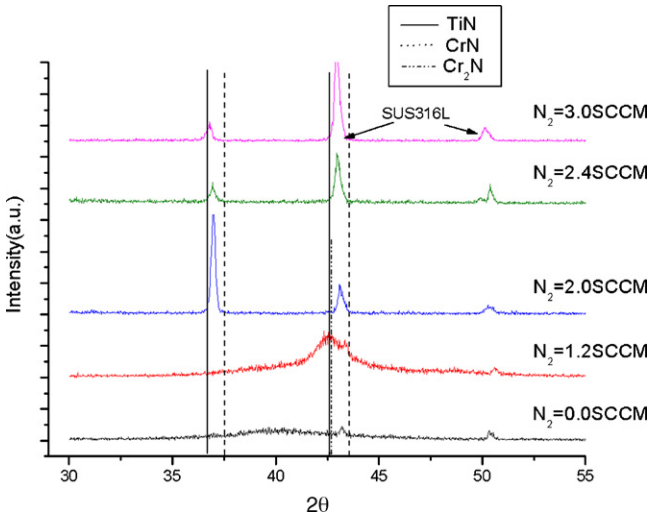

Fig. 1. XRD patterns of (Ti,Cr)N_x coatings as function of N_2 flow rate.

styrene–butadiene rubber as a binder. They showed that the interfacial contact resistance decreases significantly when there was better contact between the bipolar plate and the gas-diffusion layer. Oh and co-workers [26] also showed that the interfacial contact resistance and the contact angle of TiN coatings were comparable to those of graphite. It is known, however, that a TiN coating cannot satisfy the above-mentioned material requirements, especially the corrosion resistance, for a bipolar plate.

In this study, ternary (Ti,Cr)N_x coatings are formed on an 316L stainless-steel substrate by inductively-coupled plasma (ICP)-assisted reactive magnetron sputtering. The electrochemical and electrical properties of the coatings are investigated from the viewpoint of application in PEMFCs.

2. Experimental details

The (Ti,Cr)N_x coatings were deposited on 316L stainless-steel substrates by ICP-assisted reactive magnetron sputtering. A Ti–Cr alloy (99.9%, 2 in., Ti:Cr = 50:50 at.%) was used as the sputtering target, and the (Ti,Cr)N_x coatings were deposited using a gas mixture of Ar and N_2. The distance between the target and the substrate was 100 mm, and a two-turn copper coil (diameter = 100 mm) was

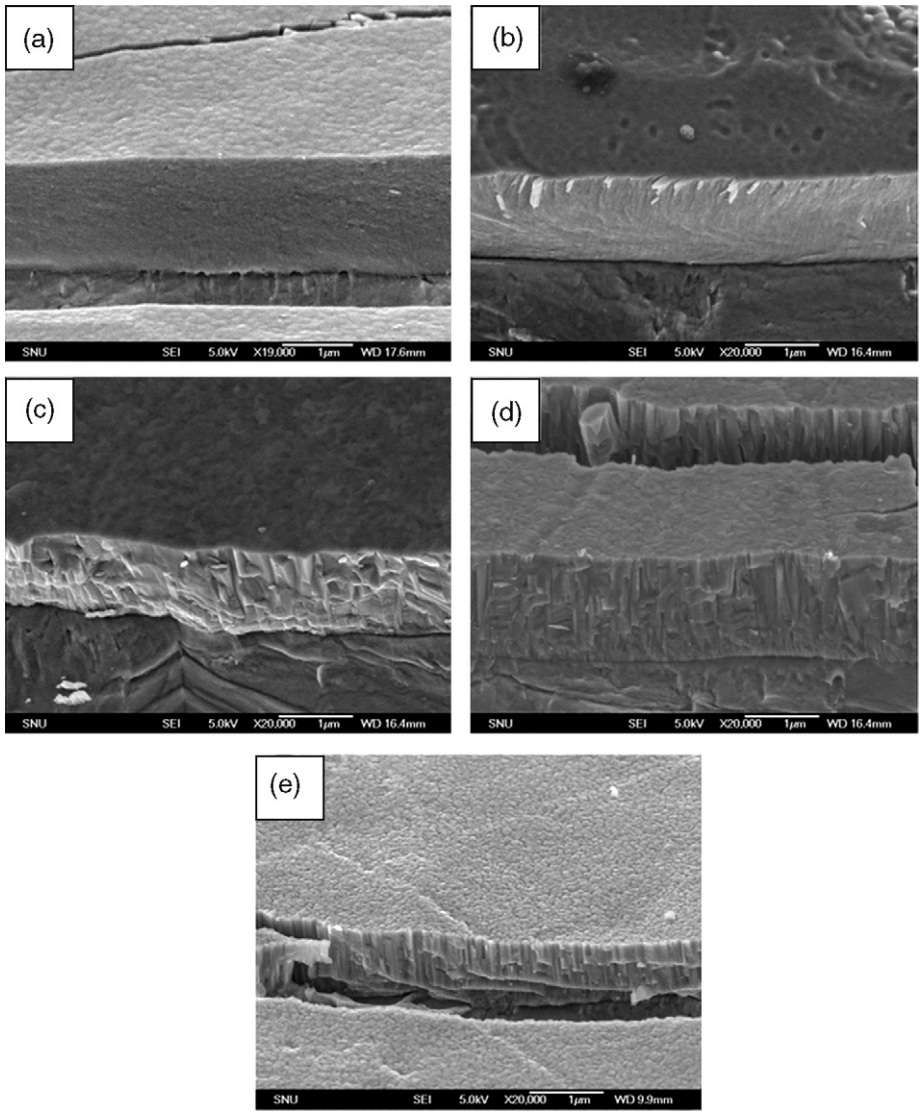

Fig. 2. FE-SEM images of (Ti,Cr)N_x coatings deposited at (a) N_2 = 0.0 sccm, (b) N_2 = 1.2 sccm, (c) N_2 = 2.0 sccm, (d) N_2 = 2.4 sccm, and (e) N_2 = 3.0 sccm.

Table 1
Deposition conditions for (Ti,Cr)N_x coatings.

DC power/W	300
RF power/W	400
Working pressure/Pa	5.32
Substrate temperature/°C	200
Ar flow rate/sccm	10
N_2 flow rate/sccm	0–3.0
Substrate bias/V	−10
Deposition rate/nm min^{-1}	41.7–58.3

located between them. The coil was shielded by means of an insulating material. The ICP was generated by applying an RF power of 13.56 MHz through a tuning network to the coil.

The base pressure of the chamber was $<5 \times 10^{-4}$ Pa prior to deposition, and the substrate temperature was maintained at 200 °C. Before deposition, the substrate was treated by ICP at 400 W, 5.32 Pa, and a substrate bias of −30 V for 4 min to remove the native oxides and impurities present on the surface. The other process conditions are listed in Table 1.

The structure of the coatings was analyzed by X-ray diffractometry (XRD) (MAC Science M18XHF-SRA) and field-emission scanning electron microscopy (FE-SEM) (JEOL JSM6330F). The cross-section of the coating could be observed by bending and cracking the film. Concentration depth profiles were obtained by Auger electron spectroscopy (AES) (Perkin-Elmer, model 670).

The corrosion property of the samples was measured in a 0.05 M H_2SO_4 + 2 ppm HF solution at 80 °C, simulating the operation conditions of a PEMFC. A conventional three-electrode system was used in the corrosion test; a carbon rod, a saturated calomel electrode (SCE), and the coated sample were used as the counter electrode, reference electrode and working electrode, respectively. Unless otherwise stated, all potentials are reported with respect to the SCE. Measurements were carried out using an AMETEK VersaSTAT3 potentiostat/galvanostat. In order to simulate a PEMFC bipolar plate, the electrolyte was purged with hydrogen gas (for an anode environment) and air (for a cathode environment). The samples were stabilized at the open-circuit potential (OCP) for 15 min. For potentiodynamic polarization, the potential scan was from −0.2 V (vs. OCP) to 1.0 V at a scanning rate of 1.5 mV s^{-1}. For potentiostatic polarization, two potentials were selected, namely: −0.1 and 0.6 V for the anode cathode environment, respectively. The total test time was 6000 s.

The Davies method was used for measurement of the interfacial contact resistance (ICR) between the sample and carbon paper (SGL 10BB) [29]. The ICR was measured with an IM6 unit (ZANHER Electrik) under compressive forces of 50, 100 and 150 N cm^{-2} that were applied with a compressor (Instron5566). Before measurement, the samples were cleaned with double-distilled water and methanol for 3 min. The ICR was calculated by subtracting R_{extra} (Eq. (2)) from R_{total} (Eq. (1)). R_{total} is the sum of all components of the resistance, and R_{extra} is measured from a single sheet of carbon paper placed between two gold-plate current-collectors without the sample.

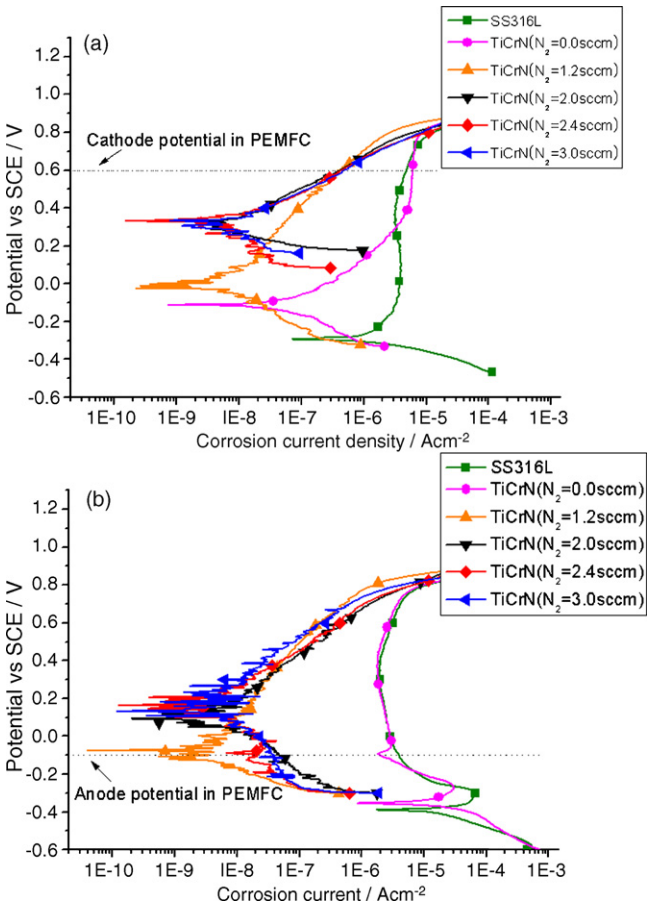

Fig. 3. Potentiodynamic polarization curve of (Ti,Cr)N_x coatings: (a) cathode condition (air bubbling); (b) anode condition (H_2 bubbling).

$$R_{total} = 2R_{coating\text{-}carbon} + 2R_{carbon-gold} + 2R_{carbon} + R_{sample} + R_{circuit} \quad (1)$$

$$R_{extra} = 2R_{carbon-gold} + 2R_{carbon} + R_{circuit} \quad (2)$$

$$R_{coating\text{-}carbon} = \frac{R_{total} - R_{extra}}{2} \quad (3)$$

where $R_{coating\text{-}carbon}$ is the interfacial contact resistance between the coating and the carbon paper; $R_{carbon-gold}$ is the interfacial contact resistance between the carbon paper and the gold-plated current-collector; R_{carbon} is the bulk resistance of the carbon paper, which is negligible; R_{sample} is the bulk resistance of the sample which is negligible; $R_{circuit}$ is the resistance of device and circuit.

3. Results and discussion

Fig. 1 shows the XRD patterns of the (Ti,Cr)N_x coatings as a function of N_2 flow rate. A broad peak is observed for the sample

Table 2
E_{corr} and current density of (Ti,Cr)N_x coatings from potentiodynamic polarization test in 0.05 M H_2SO_4 + 2 ppm HF solution at 80 °C.

	Cathode environment (air bubbling)		Anode environment (H_2 bubbling)	
	E_{corr}/V	Current density (at 0.6 V)/A cm^{-2}	E_{corr}/V	Current density (at −0.1 V)/A cm^{-2}
316L stainless-steel	−0.29	4.76×10^{-6}	−0.38	3.12×10^{-6}
TiCrN(N_2 = 0.0 sccm)	−0.11	6.09×10^{-6}	−0.41	3.26×10^{-6}
TiCrN(N_2 = 1.2 sccm)	−0.03	3.97×10^{-7}	−0.07	-1×10^{-8}, cathodic region
TiCrN(N_2 = 2.0 sccm)	0.32	4.34×10^{-7}	0.11	-2×10^{-8}, cathodic region
TiCrN(N_2 = 2.4 sccm)	0.33	4.60×10^{-7}	0.16	-5×10^{-8}, cathodic region
TiCrN(N_2 = 3.0 sccm)	0.33	4.93×10^{-7}	0.16	-3×10^{-8}, cathodic region

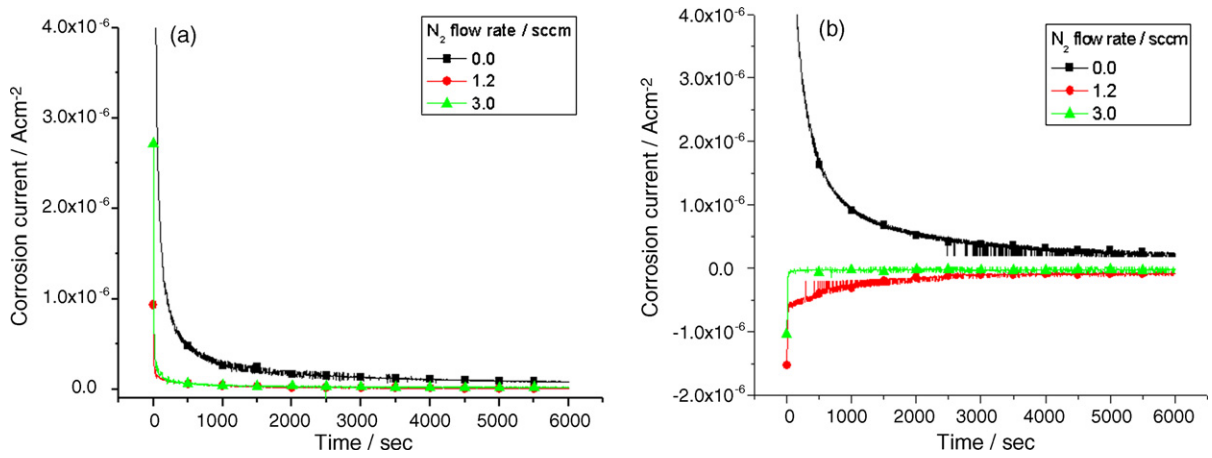

Fig. 4. Potentiostatic polarization curves of $(Ti,Cr)N_x$ coatings: (a) 0.6 V with air bubbling for cathode condition; (b) at–0.1 V with H_2 bubbling for anode condition.

deposited without nitrogen, and the grain size (calculated using Scherrer's formula) is approximately 3 nm. The β-$(Ti,Cr)_2N$ phase appears to form at a N_2 flow rate of 1.2 sccm, as reported previously by Vetter et al. [30]. The sharp peak between the TiN and CrN peaks indicates that a well-crystallized (Ti,Cr)N phase is formed when the nitrogen flow rate is ≥2.0 sccm. (Ti,Cr)N is a solid solution of TiN and CrN having the same crystal structure and similar lattice parameters of 0.424 and 0.414 nm, respectively.

The cross-sectional and surface images of the coatings as observed by FE-SEM are presented in Fig. 2. The structure of the coating changes to a columnar form with increase in the nitrogen flow rate. The coatings exhibit excellent corrosion properties even with a columnar structure.

Potentiodynamic polarization curves of the $(Ti,Cr)N_x$ coatings were measured in a 0.05 M H_2SO_4 + 2 ppm HF solution at 80 °C for bubbling with air (Fig. 3(a)) or hydrogen gas (Fig. 3(b)). Current densities at 0.6 and −0.1 V as well as the corrosion potentials (E_{corr}) are listed in Table 2. In the cathode condition, the coated samples display much better corrosion resistance than bare 316L stainless-steel. When the nitrogen flow rate is >2.0 sccm, the polarization curves have a similar pattern with very low currents at 0.6 V ($<5\times10^{-7}$ A cm^{-2}) and high corrosion potentials (>0.3 V). The corrosion current at 0.6 V is also low ($<5\times10^{-7}$ A cm^{-2}) in the 1.2 sccm sample; but the corrosion potential is not as high (0.0 V) as that of the samples coated at >2.0 sccm. In the case of the sample coated without nitrogen gas, the current density at 0.6 V (6.0×10^{-6} A cm^{-2}) decreases to the same level as that of 316L stainless-steel, and the corrosion potential also decreases to −0.11 V, although it is still higher than that of bare stainless-steel. In the anode condition, the potentiodynamic polarization curves are similar to those for the cathode condition, while the corrosion potentials decrease slightly for all samples. When the nitrogen flow rate is >1.2 sccm, the potentiodynamic polarization curves are in the cathodic region at −0.1 V and the current density is $<-1.0\times10^{-7}$ A cm^{-2}.

The corrosion potential of the $(Ti,Cr)N_x$ coatings increases with the nitrogen flow rate for both anode and cathode conditions. A comparison of this finding with the data in Fig. 1 indicates that the (Ti,Cr)N phase has the highest corrosion potential, followed by β-$(Ti,Cr)_2N$, and nanocrystallized Ti, Cr. Lee et al. [31] and Shokouhy et al. [32] reported that the corrosion potential of CrN is higher than that of Cr_2N and Cr. The corrosion potentials of Ti, Cr and their nitrides are calculated for the following simple reactions in an aqueous solution in the standard state.

$$Ti = Ti^{2+} + 2e^- \quad E = -1.63\,V$$

$$Cr = Cr^{2+} + 2e^- \quad E = -0.90\,V$$

$$2TiN = 2Ti^{2+} + N_2 + 4e^- \quad E = 0.03\,V$$

$$2CrN = 2Cr^{2+} + N_2 + 4e^- \quad E = -0.42\,V$$

Clearly, the corrosion potentials of the metal nitrides are higher (i.e., more positive) than those of the pure metals.

Fig. 4 shows potentiostatic polarization measurements for the $(Ti,Cr)N_x$ samples coated at 0.6 V with air bubbling (Fig. 4(a)) and at −0.1 V with H_2 bubbling (Fig. 4(b)). In the cathode condition, all the coated samples stabilize at a low current density of around 1×10^{-7} A cm^{-2}. In the anode condition, the (Ti,Cr)N and β-$(Ti,Cr)_2N$ coatings exhibit a negative current density because they

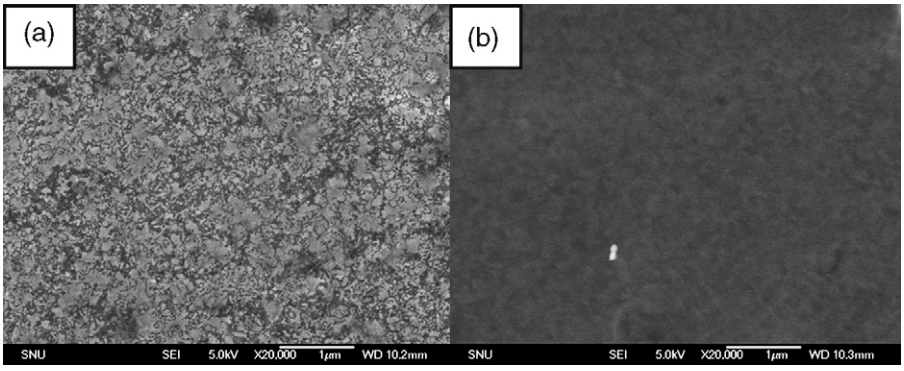

Fig. 5. Surface image of coatings deposited at (a) N_2 = 0.0 sccm and (b) N_2 = 3.0 sccm after potentiostatic polarization test for anode condition (H_2 bubbling).

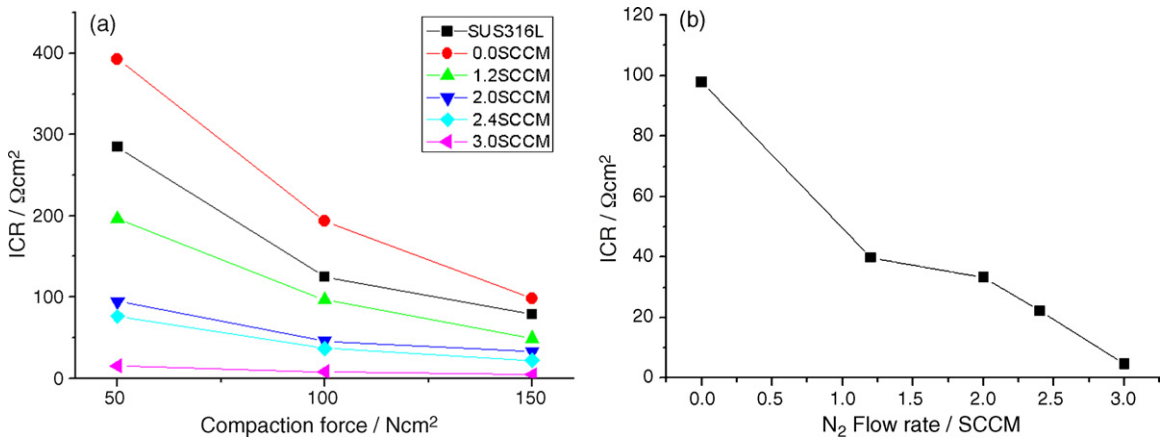

Fig. 6. ICRs of (Ti,Cr)N_x coatings as function of compaction force and nitrogen flow rate.

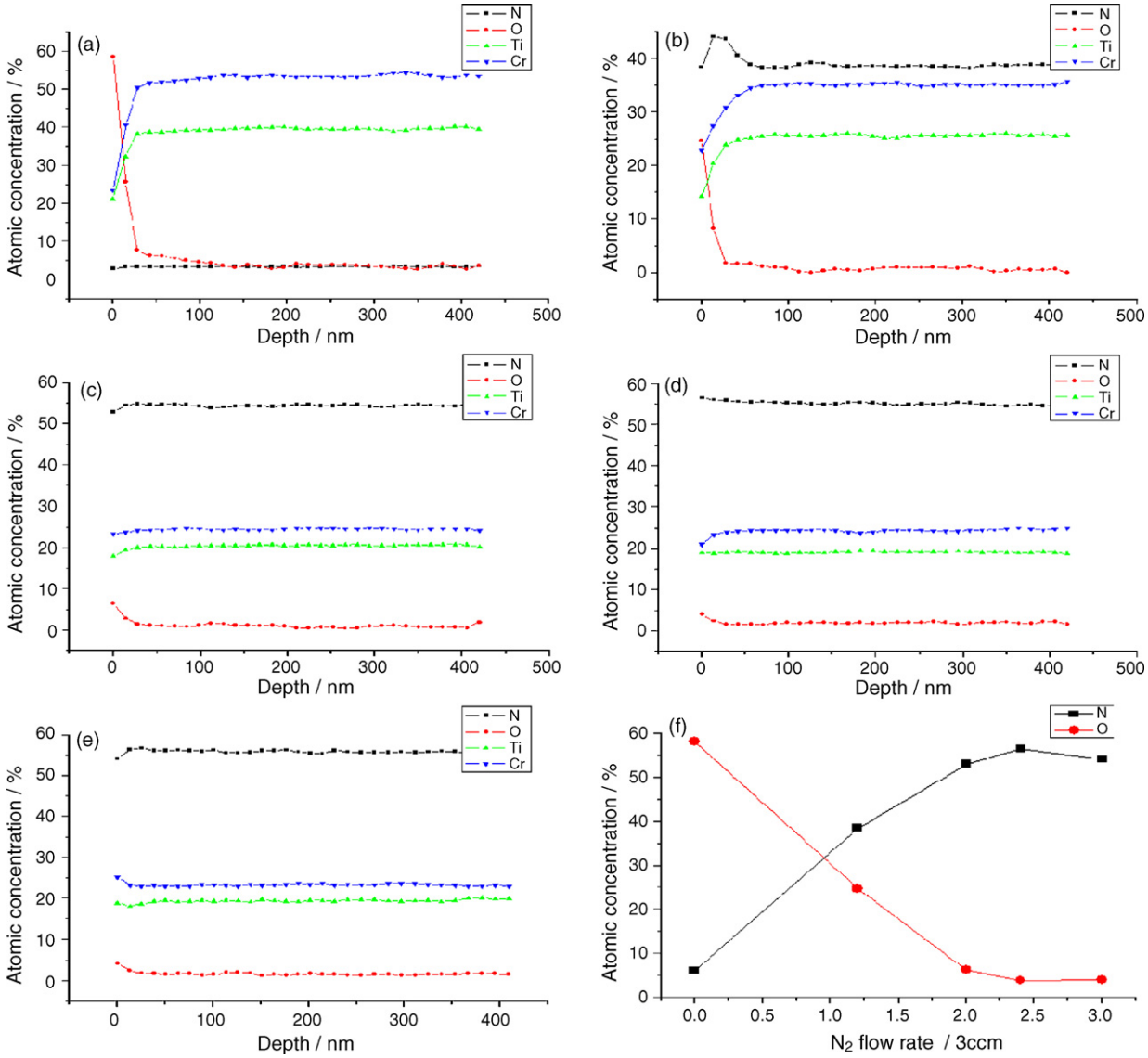

Fig. 7. Concentration depth profiles of TiCrN coatings deposited at (a) N_2 = 0.0 sccm, (b) N_2 = 1.2 sccm, (c) N_2 = 2.0 sccm, (d) N_2 = 2.4 sccm, (e) N_2 = 3.0 sccm, and (f) oxygen and nitrogen concentrations on surface.

have a corrosion potential higher than −0.1 V. The negative current implies that the (Ti,Cr)N coatings act as a cathodic protection material without dissolution. On the other hand, positive current is observed for the Ti–Cr-coated sample.

Surface images of the coatings after potentiostatic polarization tests in the anode condition (H_2 bubbling) and for deposition at N_2 = 0.0 sccm and N_2 = 3.0 sccm are shown in Fig. 5(a) and (b), respectively. There is no change in the surface morphology at N_2 = 3.0 sccm, whereas a corroded surface is be observed at N_2 = 0.0 sccm.

The ICRs of the (Ti,Cr)N_x coatings are presented in Fig. 6. The ICR decreases with increase in the compaction force and the nitrogen flow rate. As is well known, the this influence of the compaction force is due to an enlargement of the actual contact area. When the nitrogen flow rate is ≥2.0 sccm, the ICR value of the (Ti,Cr)N coating is lower than that of 316L stainless-steel. The minimum value is 4.5 mΩ cm^2 at a compaction force of 150 N cm^{-2} for a coating produced at N_2 = 3.0 sccm. Fig. 7 shows the concentration depth profiles of Ti, Cr, N, and O as a function of nitrogen flow rate. The oxygen concentration on the surface of the coatings decreases with increase in nitrogen concentration (Fig. 7(f)). The thickness of the oxide layer also decreases with increase in nitrogen flow rate. This shows that the formation of the oxide layer at the surface can be prevented by nitride formation owing to the strong covalent bonding between the metal and nitrogen.

4. Conclusion

The (Ti,Cr)N_x coatings are deposited on 316L stainless-steel substrates by inductively-coupled, plasma-assisted, magnetron sputtering. The chemical and electrical properties are investigated from the viewpoint of applications to bipolar plates. At a low N_2 flow rate of 1.2 sccm, a hexagonal β-$(Ti,Cr)_2N$ phase is observed, while a (Ti,Cr)N phase is formed at N_2 >2.0 sccm. It is found that the (Ti,Cr)N coating exhibits the highest corrosion potential and lowest current density. In the simulated cathode condition, the corrosion potential and current density are 0.33 V and $<5 \times 10^{-7}$ A cm^{-2} (at 0.6 V), respectively, whereas they are 0.16 V and $<-5 \times 10^{-8}$ A cm^{-2} (cathodic region) in the simulated anode condition. The (Ti,Cr)N coatings exhibit excellent stability during potentiostatic polarization testing in both anode and cathode environments.

The ICR values of the (Ti,Cr)N-coated sample are lower than that of bare 316L stainless-steel, with a minimum value of 4.5 mΩ cm^2 at a compaction force of 150 N cm^{-2}. Analysis with AES shows that the oxygen content on the surface of the coating and the thickness of the oxide layer are both reduced with increase in nitrogen concentration. The (Ti,Cr)N coating serves as a barrier coating that prevents corrosive media from penetrating the substrate; further, it prevents oxide formation at the coating surface.

Acknowledgements

The authors are grateful for financial support provided by Hyundai HYSCO Corp. and the Fundamental R&D program for Core Technology of Materials (M-2007-01-0006) funded by the Ministry of Commerce, Industry and Energy, Republic of Korea.

References

[1] S.G. Chalk, P.G. Patil, S.R. Venkateswaran, J. Power Sources 61 (1996) 7–13.
[2] B.C.H. Steele, A. Heinzel, Nature (London) 414 (2001) 345–352.
[3] S.J.C. Cleghorn, X. Ren, T. Espringer, M.S. Wilson, C. Zawodzinski, T.A. Azwodzinski, S. Gottesfeld, Int. J. Hydrogen Energy 22 (1997) 1137–1144.
[4] J. Ihonen, F. Jaouen, G. Lindbergh, G. Sundholm, Electrochim. Acta 46 (2001) 2899–2911.
[5] H. Tsuchiya, O. Kobayashi, Int. J. Hydrogen Energy 29 (2004) 985–990.
[6] K.S. Jeong, B.S. Oh, J. Power Sources 105 (1) (2002) 58–65.
[7] M.P. Brady, K. Weisbrod, C. Zawodzinski, I. Paulauskas, R.A. Buchanan, L.R. Walker, Electrochem. Solid State Lett. 5 (11) (2002) A245–A247.
[8] M.P. Brady, K. Weisbrod, I. Paulauskas, R.A. Buchanan, K.L. More, H. Wang, M. Wilson, F. Garzon, L.R. Walker, Scripta Mater. 50 (7) (2004) 1017–1022.
[9] H. Wang, M.P. Brady, K.L. More, H.M. Meyer III, J.A. Turner, J. Power Sources 138 (1–2) (2004) 79–85.
[10] I.E. Paulauskas, M.P. Brady, H.M. Meyer III, R.A. Buchanan, L.R. Walker, Corrosion Sci. 48 (10) (2006) 3157–3171.
[11] M.P. Brady, H. Wang, B. Yang, J.A. Turner, M. Bordignon, R. Molins, M. Abd Elhamid, L. Lipp, L.R. Walker, Int. J. Hydrogen Energy 32 (16) (2007) 3778–3788.
[12] H. Wang, J.A. Turner, M.P. Brady, ECS Transactions 11 (1 part 2) (2007) 1461–1471.
[13] E.S. Puchi Cabrera, Mater. Sci. Technol. 17 (2001) 155–161.
[14] S. Venugopal, S.L. Mannan, Y.V.R.K. Prasad, Scripta Metal. Mater. 28 (6) (1993) 715–720.
[15] J. Takada, Y. Ohizumi, H. Miyamura, H. Kuwahara, S. Kikuchi, I. Tamura, J. Mater. Sci. 21 (1986) 2493–2496.
[16] P.A. Dearnley, A. Namvar, G.G.A. Hibberd T. Bell, Some observations on plasma nitriding austenitic stainless steels (1989) Plasma Surface Engineering, 1, pp. 219–226.
[17] Y. Fu, M. Hou, H. Xu, Z. Hou, P. Ming, Z. Shao, B. Yi, J. Power Sources 182 (2) (2008) 580–584.
[18] Y. Fu, M. Hou, D. liang, X. Yan, Y. Fu, Z. Shao, Z. Hou, P. Ming, B. Yi, Carbon 46 (1) (2008) 19–23.
[19] Y. Show, Surf. Coat. Technol. 202 (4–7) (2007) 1252–1255.
[20] S.-H. Wang, J. Peng, W.-B. Lui, J.-S. Zhang, J. Power Sources 162 (1) (2006) 486–491.
[21] W.-S. Jeon, J.-G. Kim, Y.-J. Kim, J.-G. Han, Thin Solid Films 516 (11) (2008) 3669–3672.
[22] Y. Wang, D.O. Northwood, J. Power Sources 165 (1) (2007) 293–298.
[23] W.-Y. Ho, H.-J. Pan, C.-L. Chang, D.-Y. Wang, J.J. Hwang, Surf. Coat. Technol. 202 (4–7) (2007) 1297–1301.
[24] M. Li, S. Luo, C. Zeng, J. Shen, H. Lin, C. Cao, Corrosion Sci. 46 (6) (2007) 1369–1380.
[25] S.-T. Myung, M. Kumagai, R. Asaishi, Y.-K. Sun, H. Yashiro, Electrochem. Commun. 10 (3) (2008) 480–484.
[26] E.A. Cho, U.-S. Jeon, S.-A. Hong, I.-H. Oh, S.-G. Kang, J. Power Sources 142 (1–2) (2005) 177–183.
[27] H. Wang, J.A. Turner, X. Li, G. Teeter, J. Power Sources 178 (1) (2008) 238–247.
[28] H. Wang, J.A. Turner, J. Power Sources 170 (2) (2007) 387–394.
[29] D.P. Davies, P.L. Adcock, M. Turpin, S.J. Rowen, J. Appl. Electrochem. 30 (2000) 101–105.
[30] J. Vetter, H.J. Scholl, O. Knotek, Surf. Coat. Technol. 74–75 (1995) 286.
[31] K.H. Lee, C.H. Park, Y.S. Yoon, J.J. Lee, H.A. Jehn, J. Vac. Sci. Technol. A 19 (5) (2001) 2504–2513.
[32] A. Shokouhy, M.M. Larijani, M. Ghoranneviss, S.H. Haji Hosseini, G.M. Yari, A.H. Sari, M. Gholipur Shahraki, Thin Solid Films 515 (2 SPEC ISS.) (2006) 571–575.